

OPTIMIZATION OF PROCESS PARAMETERS IN FRICTION STIR WELDING OF DISSIMILAR ALUMINUM ALLOYS: INSIGHTS INTO WELD QUALITY AND TOOL WEAR DYNAMICS

Ibrahim Sabry

**Department of Mechanical Engineering, Benha Faculty of Engineering,
Benha University, Benha, 13511, EGYPT.**

ABSTRACT

Abstract Friction stir welding (FSW) is a solid-state joining technique known for combining two workpieces through pressure and intense plastic deformation, avoiding melting. This method offers advantages such as lower energy consumption, enhanced mechanical properties, and reduced defects compared to traditional fusion welding techniques. The performance of FSW is highly influenced by key process parameters, including rotational speed, travel speed, and tilt angle, which govern critical outcomes such as maximum Temperature, ultimate tensile strength (UTS), and tool wear. This study investigates the interplay between these parameters in joining dissimilar aluminum alloys, 6061-T6 and 6082-T6. Using Response Surface Methodology (RSM), a robust statistical approach, the research optimizes and analyzes the relationships among the process parameters and their effects on weld quality and tool wear. Novel insights are presented regarding the linear relationship between tool wear and rotational speed and the inverse relationships with travel speed and tilt angle. Notably, higher rotational speeds increased tool wear while concurrently reducing tool surface roughness, highlighting the trade-offs in parameter selection.

Furthermore, the study identifies optimal FSW conditions to achieve a maximum temperature of 737°C, corresponding to a rotational speed of 2000 rpm, a travel speed of 10 mm/min, and a tilt angle 2°. These optimal settings improve weld quality and minimize tool wear, providing practical guidance for industrial applications. By focusing on the combined effects of rotational speed, travel speed, and tilt angle, this research fills a critical gap in understanding the simultaneous Optimization of weld quality and tool longevity in FSW of dissimilar aluminum alloys.

KEYWORDS

FSW, dissimilar aluminum, rotation speed, tool wear, Temperature, UTS.

INTRODUCTION

FSW is a solid-state joining method that joins two work pieces by applying pressure and substantial plastic deformation around their melting temperatures, [1]. Friction

Stir Welding (FSW) presents numerous advantages over alternative methods, including lower energy consumption, less residual stress, enhanced mechanical properties, fewer defects, and environmentally sustainable attributes, [2]. This approach is utilized to amalgamate materials that are both analogous and disparate. The creation and proper distribution of heat are the principal factors in achieving optimal and defect-free bonding in the FSW process. The generation of heat in FSW results from the synergistic effects of friction and plastic deformation, as noted by, [3]. Mishra et al., [4] assert that the principal cause of heat generation in machining processes is the friction between the tool and the work piece. Separate zones in workpieces are created due to the uneven heat dispersion in FSW. The noted differences among these places can be ascribed to plastic deformations, thermal distributions, residual stresses, and variations in the microstructure. In Friction Stir Welding with different materials, the meticulous control of heat distribution is critically important. The substantial asymmetry in heat distribution at the joints is due mainly to the mechanical and thermal characteristics of the relevant materials. To alleviate this limitation, it is essential to displace the tool from the weld line, [5]. Essa et al., [6] indicate that the offsetting pin from the shoulder technique is innovative for attaining equal heat distribution in workpieces. Displacing the pin increases the flow of plastic material inside a fixed pin volume, expanding the welded cross-section area. A multitude of studies has been undertaken with tool offsetting.

Ramachandran et al., [7] examined the Effect of tool offset distance on the mechanical characteristics and microstructures of steel and aluminum alloy during FSW. The findings indicate that the offset distance significantly influences the mechanical characteristics and microstructures. Khan et al., [8] examined the impact of tool offset distance and shoulder penetration on defects in the FSW process of AA5083 and AA6063-T6. It was found that transitioning towards more excellent ductility efficiently mitigates tunnel defects and significantly enhances ultimate tensile strength (UTS). Shah et al., [9] investigated the Influence of the eccentricity tool on the flow of material through the FSW of AA6061. Their findings suggested that the implementation of offsetting led to an increase in both the material flow and the weld area. Naghibi et al., [10] examined the Influence of tool offsets on the ultimate tensile strength of weld joints composed of AA5052 and AISI 304. The researchers utilized a genetic algorithm to enhance UTS.

Liang et al., [11] investigated the impact of process parameters and offset of tools on the mechanical characteristics of the weld junction between aluminum and magnesium alloys, explicitly targeting the advancing side. Research indicates that varying rotating speeds reduce UTS when combined with offsetting towards aluminum or magnesium alloy. Sahu et al., [12] sought to investigate the factors influencing dissimilar FSW metals. The research conducted by R. Srinivasan et al., [12] examined the impact of offsetting on the flow of material through FSW of aluminum and titanium. The study demonstrated that axial forces substantially increase material flow. In this study, Sabry et al., [13] examined the Influence of process parameters, rotation speed, and travel speed on defect formation during FSW of 6061 aluminum alloy. The study's findings demonstrate that the tool offset significantly influences the mechanical properties of the weld. Marathe Shalin et al., [14] enhanced the mechanical qualities of a joint created using FSW of AA6061 in

their Investigation. This was accomplished by analyzing the effects of tool rotation velocity and tool pin configuration.

P. Sevel et al., [15] examined the Influence of axial force and tool shape on the mechanical characteristics of AZ80A Mg alloy in an advancing side weld joint. Their Investigation sought to ascertain the optimal value of axial force. Sabry et al., [16] examined the effects of rotation speed, clamping torque, and clamping pitch on the mechanical properties of the weld joint between AA6061, with a specific emphasis on the advancing side. The greatest ultimate tensile strength (UTS) is achieved with a Clamp Pitch of 30 mm, a rotational speed of 1800 rpm, and a Clamping Torque of 70 Nm. M. Rethmeier et al., [17] examined the Influence of four different traverse forces, axial force, and tool torque on the FSW process of AA2024-T4. The researchers determined the ideal offset that enhanced the weld area and improved the microstructure and mechanical qualities of the welded material. Mouminah Amatullah et al., [18] examined the impact of rotational speed on several aluminum alloys' mechanical and microstructural characteristics. The impact of process factors, like the speed of rotation, speed of traverse, and geometry of the tool, is essential for producing defect-free welds and improving joint efficiency. Moreover, the material's placement affects the mechanical properties of the joint, temperature distribution, and plastic flow, in addition to the previously mentioned parameters of tool offset and pin offset, [19]. The material location plays a crucial role in influencing a joint's temperature distribution, mechanical properties, and microstructure due to the asymmetry of plastic flow on both sides of the weld line, [20]. Over the past fifteen years, numerous studies have investigated dissimilar aluminum alloy joints' friction stir welding (FSW), concentrating on process optimization and the Influence of process parameters, microstructure, mechanical properties, and heat treatments, [21 - 27]. Extensive research has been undertaken on the FSW of dissimilar metals; nevertheless, the impact of material positioning on temperature distribution and peak temperature has been inadequately explored.

This study examines the simultaneous effects of rotation speed, travel speed, and tilt angle on process temperature in dissimilar FSW of 6061-T6 and 6082-T6 aluminum alloys. Novel experimental procedures that have not been previously applied are utilized. The research used Response Surface Methodology (RSM) to assess the Influence of the three variables on maximum Temperature, UTS, and tool wear rate in the process.

Materials and Methods

Material

This work employed two specific aluminum alloys, 6061-T6 and 6082-T6, to perform the FSW process.

Table 1 Displays the weight percentages of the chemical compositions of two aluminum alloys, specifically 6061-T6 and 6082-T6.

Weight (%)	Al	Si	Fe	Cu	Mn	Mg	Zn	Ti	Cr
AA6082alloy	Balance	1.2	0.5	0.1	1.0	1.2	0.2	0.1	0.25
AA6061 alloy	Balance	0.80	0.70	0.40	0.15	0.80	0.25	0.15	0.35

Table 2 Details the mechanical properties of 6061-T6 and 6082-T6 alloys.

	Ultimate Tensile Strength	Elongation (%)	Vickers Hardness
AA6061-T6	290	10	95
AA6082-T6	320	12	110

Table 3 Details of the mechanical properties of SS316.

	Ultimate Tensile Strength	Yield Strength (MPa)	Vickers Hardness
SS316	480	175	95

This procedure produced two workpieces measuring $100 \times 70 \times 6 \text{ mm}^3$ for Welding. A tool constructed from SS316L was employed for FSW. The mechanical characteristics of SS316L are presented in Table 3.

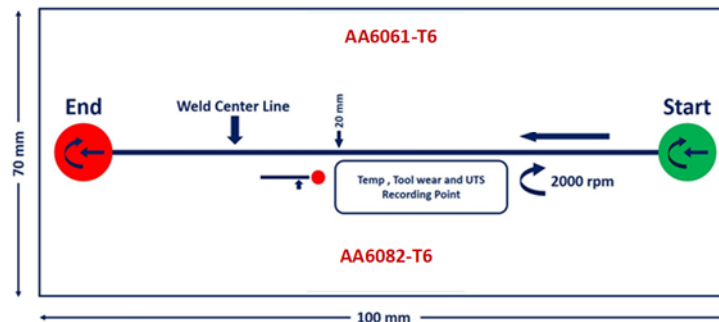


Fig. 1 The process flow diagram for Friction Stir Welding (FSW).

The geometric proportions are depicted in Figure 2. The conical pin was designed to enable the effortless insertion of the tool into the samples during the piercing procedure. As a result, the FSW tool was constructed according to the geometric specifications detailed in Table 4.

Table 4 The geometric dimensions of the FSW tool pertain to its physical features.

Tool of length	45
Pin diameter (tip)	0.9 mm
Pin length	2.9mm
Pin diameter (shoulder near)	1.9 mm
Shoulder diameter	10 mm

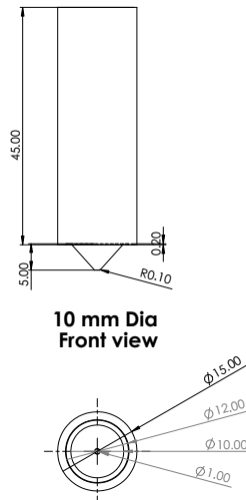


Fig. 2 Tool geometric dimensions.

The FSW procedure was performed using a milling machine, and an appropriate fixture was created before examining five examples. An infrared thermometer was attached to the mobile component of the milling machine to assess the Temperature of welded samples, ensuring they traveled at the same velocity as the FSW travel speed. The temperature history at a point 15 mm from the weld line on the advancing side was documented during each FSW treatment, as seen in Figure 1. Figure 3 illustrates the welding apparatus and thermometer. Moreover, Figure 4 illustrates welded specimens employing five different procedures.



Fig. 3 FSW Configuration.

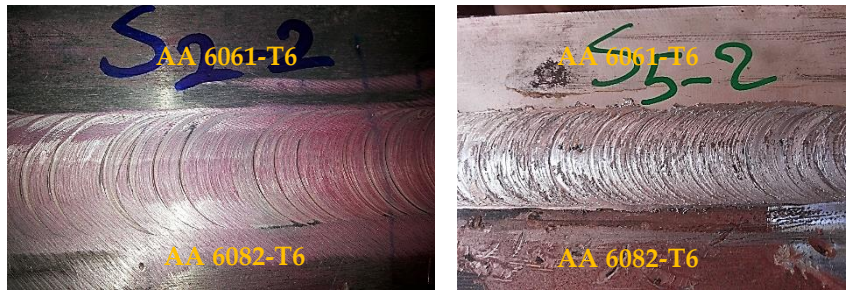


Fig. 4 Specimens fused with diverse instruments.

2.2 Tensile test

Three tensile specimens were produced for each experiment by the ASTM E8M-04 standard. The UTS of the FSW joints was assessed using a universal testing apparatus. The acquired data, comprising three measurements, is summarized in Figure 5, illustrating the average values.

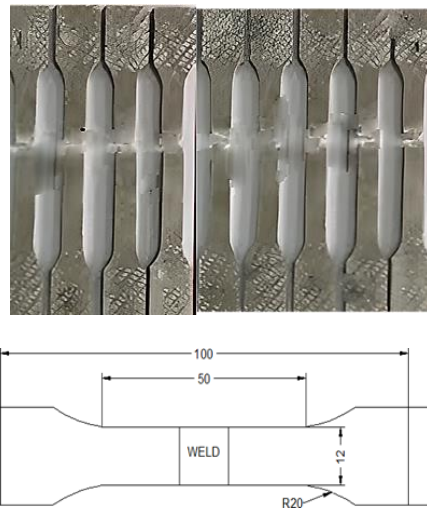


Fig. 5 The tensile test specimen, with all dimensions expressed in millimeters.

Temperature

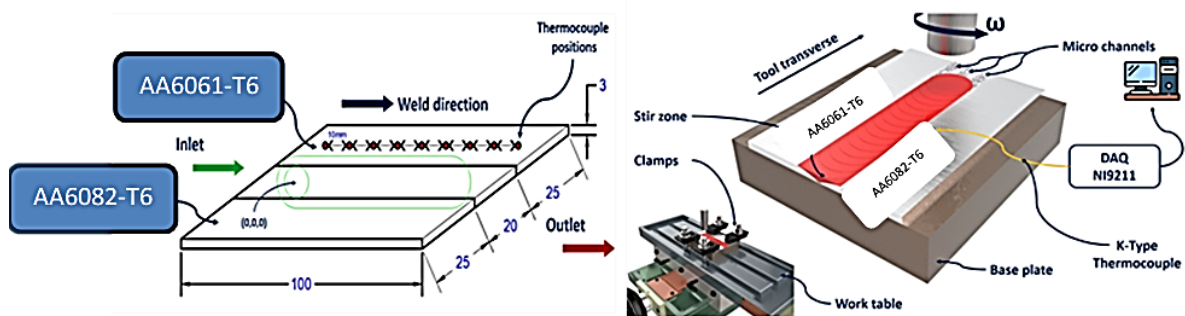


Fig. 6 The thermocouple's position is depicted schematically.

Two thermocouples of type-K were utilized to measure the temperatures at 3 mm places along the specimen's lateral axis from the weld line. The objects above were meticulously positioned within pre-drilled cavities of 1 mm diameter and 1 mm depth, situated on the underside of the plate component. Figure 6. presents a schematic representation of the spatial configuration of the thermocouples. Statistical analysis was performed utilizing the mean temperature value. The specimen used for tensile testing is defined by its dimensions and measured in millimeters.

Tool wear

A tool's wear resistance can be assessed by quantifying the mass and volume loss incurred. The effects of these parameters are evaluated. The tool's Wear is measured by measuring the weight reduction of each tool steel post-FSW. This study quantifies tool wear by measuring the weight reduction of tool steels following the friction stir welding (FSW) technique applied to AA6061-T6 and AA6082-T6 plates. The mass of the tool steel specimen is ascertained before conducting FSW with a precision scale that measures three decimal places in grams (g). The tool's weight is then calculated using the same balance after the completion of FSW. The spindle speed for FSW is set at three levels: 1000, 1500, and 2000 rpm. The tool travel speed is established at 10 and 30 mm/min, while the tilt angle is exerted at 1, 1.5, and 2 C, as seen in the schematic representation of tool wear in Fig. 7. These parameter settings are selected to provide enough heat generation for material plasticization and to reduce the likelihood of tool failure. The weight loss and percentage wear for each SS316L tool are displayed in Table 6. The % wear is calculated using Equation 1, where m_i is the original mass of the SS316L tool, and Δm indicates the change in the tool's mass.

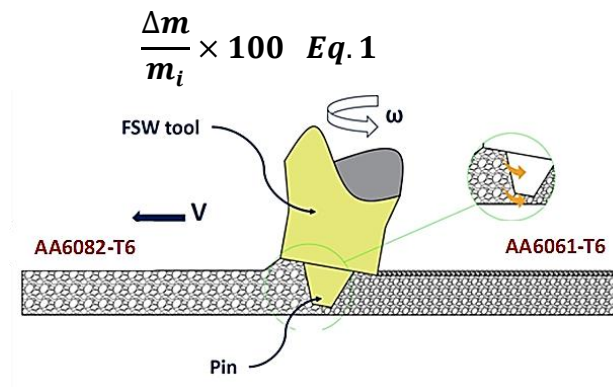


Fig. 7 Schematic depiction of tool wear.

Design of experiments (DOE)

Upon validating the numerical model, this work clarifies the experimental design utilized. This study investigated three variables: speed of rotation, speed of travel, and tilt angle, as quantitative inputs, alongside the position of alloys as qualitative inputs. The parameters of interest were the maximum Temperature, UTS, and wear rate during the operation. The maximum Temperature in the process of FSW was reached adjacent to the weld line and the base of the tool's shoulder. Temperature can be quantified via thermocouples. The Central Composite Design (CCD) analyzed the main effects and interactions. The MINITAB software utilized this approach to

conduct variance analysis (ANOVA), [28]. The study examined each quantitative variable over five unique levels, whereas the qualitative variable was intended to have two levels. Table 5 illustrates the input variables together with their respective levels.

Table 5 The tires of the input variables

Process Parameters	Unit	Symbol	Levels		
			-1	0	1
N	RPM	N	1000	1500	2000
S	mm/min	S	10	16	30
T	degree	T	1	1.5	2

RESULTS AND DISCUSSION

Results of the Experiment

A Central Composite Design (CCD) methodology was utilized to assess the Influence of major components and their interactions on the maximum Temperature of a specific process, [29]. A second-order polynomial was employed to model the maximum Temperature. A design matrix was constructed, and its specifications are delineated in Table 6. Additionally, Table 6 displays the specified output variables, precisely the maximum temperatures.

Table 6 Design matrix and output parameters.

Run	FSW process parameters			Responses		
	N	S	T	Temperature	UTS	Tool wear
1	2000	30	1.0	688.391	293.190	0.918743
2	1500	30	1.0	639.804	278.121	0.800432
3	1000	30	1.0	591.217	263.053	0.787898
4	2000	16	1.0	704.847	297.492	0.987977
5	1500	16	1.0	656.260	282.423	0.895980
6	1000	16	1.0	607.673	267.356	0.745950
7	2000	10	1.0	737.759	306.096	0.818743
8	1500	10	1.0	689.172	291.027	0.700432
9	1000	10	1.0	640.596	275.959	0.687898
10	2000	30	1.5	685.135	287.243	0.287977
11	1500	30	1.5	636.548	272.173	0.225980
12	1000	30	1.5	587.961	257.106	0.205950
13	2000	16	1.5	701.591	291.545	0.618743
14	1500	16	1.5	653.004	276.477	0.564320
15	1000	16	1.5	604.417	261.408	0.587898
16	2000	10	1.5	734.514	300.149	0.587977
17	1500	10	1.5	685.927	285.081	0.425980
18	1000	10	1.5	637.340	270.012	0.412595
19	2000	30	1.5	681.879	281.295	0.405950
20	1500	30	2.0	633.303	266.228	0.418743
21	1000	30	2.0	584.716	251.159	0.364320

22	2000	16	2.0	698.346	285.597	0.387898
23	1500	16	2.0	649.759	270.529	0.387977
24	1000	16	2.0	601.172	255.460	0.225980
25	2000	10	2.0	734.514	300.149	0.212595
26	1500	10	2.0	682.671	279.134	0.205950
27	1000	10	2.0	634.084	264.066	0.135950

In statistical analyses, R-squared and adjusted R-squared metrics are employed to evaluate the accuracy of a polynomial model. A closer closeness to unity for these metrics signifies enhanced accuracy. The statistical values of the parameters are shown in Table 8.

Table 7 displays the coefficients of the statistical model.

	UTS				
Source	Sequential p-value	Lack of Fit P-value	Adjusted R ²	Predicted R ²	
Linear	< 0.0001	0.9970	0.9891	0.9929	Suggested
	Temperature				
Linear	< 0.0001	0.1700	0.9487	0.9393	Suggested
	Wear rate				
Linear	< 0.0001	0.5362	0.8115	0.6730	

The reliability factor was determined at a confidence level of 95 %. The analysis of variance (ANOVA) technique was utilized, and the findings are displayed in Table 8. The effectiveness of each variable was evaluated according to its P value, which must be below 5% to provide a reliability level of 95%. The coefficients were chosen according to the P values displayed in Table 8. Multiple assessments were conducted to validate the fitted model, including evaluating data, normality examining variance stability across various levels, and assessing data independence over time. Table 9 presents the regression equations for maximum Temperature, UTS, and tool wear rate in FSW as functions of the relevant parameters.

Table 8 ANOVA of the considered model.

UTS						
Source	Sum of Square	df	Mean Square	F-value	p-value	
Model	5687.86	9	631.98	262.96	< 0.0001	significant
A-Rotation speed	3752.81	1	3752.81	1561.48	< 0.0001	
B-Travel speed	872.04	1	872.04	362.84	< 0.0001	
C-Tilt angle	479.48	1	479.48	199.50	< 0.0001	
AB	10.03	1	10.03	4.17	0.0569	

AC	1.70	1	1.70	0.7060	0.4125	
BC	2.86	1	2.86	1.19	0.2903	
A ²	52.15	1	52.15	21.70	0.0002	
B ²	143.14	1	143.14	59.56	<	0.0001
C ²	2.79	1	2.79	1.16	0.2965	
Residual	40.86	17	2.40			
Lack of Fit	23.17	16	1.45	0.0819	0.9970	not significant
Pure Error	17.69	1	17.69			
Cor Total	5728.7	26				
	1					
Temperature						
Source	Sum of Square	df	Mean Square	F-value	p-value	
Model	54529.03	9	6058.78	8413.68	<	significant
A-Rotation speed	39357.12	1	39357.12	54654.23	<	0.0001
B-Travel speed	10766.85	1	10766.85	14951.66	<	0.0001
C-Tilt angle	143.26	1	143.26	198.94	<	0.0001
AB	3.00	1	3.00	4.16	0.0571	
AC	0.5128	1	0.5128	0.7122	0.4104	
BC	0.8531	1	0.8531	1.18	0.2916	
A ²	552.75	1	552.75	767.59	<	0.0001
B ²	1892.56	1	1892.56	2628.15	<	0.0001
C ²	0.8473	1	0.8473	1.18	0.2932	
Residual	12.24	17	0.7201			
Lack of Fit	6.94	16	0.4338	0.0818	0.9970	not significant
Pure Error	5.30	1	5.30			
Tool wear rate						
Model	1.46	9	0.1618	13.44	<	significant
A-Rotation speed	0.0358	1	0.0358	2.98	0.1026	
B-Travel speed	0.0000	1	0.0000	0.0025	0.9609	
C-Tilt angle	1.03	1	1.03	85.28	<	0.0001
AB	0.0098	1	0.0098	0.8149	0.3793	
AC	0.0128	1	0.0128	1.06	0.3169	

BC	0.0022	1	0.0022	0.1830	0.6742	
A ²	0.0009	1	0.0009	0.0735	0.7896	
B ²	0.1004	1	0.1004	8.34	0.0102	
C ²	0.0796	1	0.0796	6.62	0.0198	
Residual	0.2046	17	0.0120			
Lack of Fit	0.1977	16	0.0124	1.78	0.5362	significant
Pure Error	0.0070	1	0.0070			
Cor Total	1.66	26				

Table 9: The conclusive regression equations for the maximum process temperature, UTS, and minimum tool wear.

UTS	=	$+259.05239+0.068426N-2.67306S-20.07559T-0.000183N * S+0.001633N * T-0.104747S * T-0.000012 N^2+0.059796 S^2+2.75299T^2$
Temperature	=	$+560.02519+0.218964N-10.96688S -11.02163T-0.000100 N* S+0.000898N * T-0.057180S * T-0.000040 N^2+0.217429 S^2+1.51777T^2$
Tool wear%	=	$+1.10985+0.000573N+0.067711S-1.77172T-5.73029E-06 N * S-0.000142N * T+0.002906S * T-5.11087E-08 N^2-0.001584S^2+0.465325T^2$

The principal components and their interconnections

The analysis of variance (ANOVA) and the connections in Table 9 indicate that all variables directly influence maximum Temperature, UTS, and tool wear percentage. The statistical analysis in Table 8 demonstrates that the F and P values reveal a considerable impact of rotation speed on maximum Temperature, UTS, and tool wear. Rotation speed notably influences maximum Temperature, followed by tilt angle, while exerting the least Effect on tool wear. Figure 8 depicts the correlation between maximum Temperature, rotation speed, travel speed, and tilt angle.

Figure 9 (a) reveals a substantial reduction in the maximum Temperature. Moreover, this reduction becomes increasingly evident at higher travel speeds. Increased travel speed within a constant volume increases the plastic flow in a larger working area. The increase in travel speed enhances plastic flow while concurrently reducing plastic flow concentration in the central region of the welded cross-section. The decrease in concentration leads to heat dissipation produced by friction and plastic flow over a broader surface area, lowering the workpiece's maximum Temperature. A study by Mourad et al., [30] made a similar result. Figure 9 (b) indicates that augmenting the travel speed in either the advancing or retreating direction diminishes the maximum Temperature. Moreover, this reduction is more significant when the tool rotation speed is oriented towards the advancing side. The rotation speed of the tool produces non-homogeneous and non-uniform flow due to an imbalance in plastic flow, resulting in a subsequent reduction in the maximum Temperature. Reduced plastic flow is noted on the advancing side due to the opposite rotational and travel speeds of the counter mechanism, in contrast to the retreating side. Consequently, a more significant reduction in plastic flow occurs when the tool's travel speed escalates

towards the advancing side. Thus, this diminution in material flow results in a more pronounced fall in the Maximum Temperature.

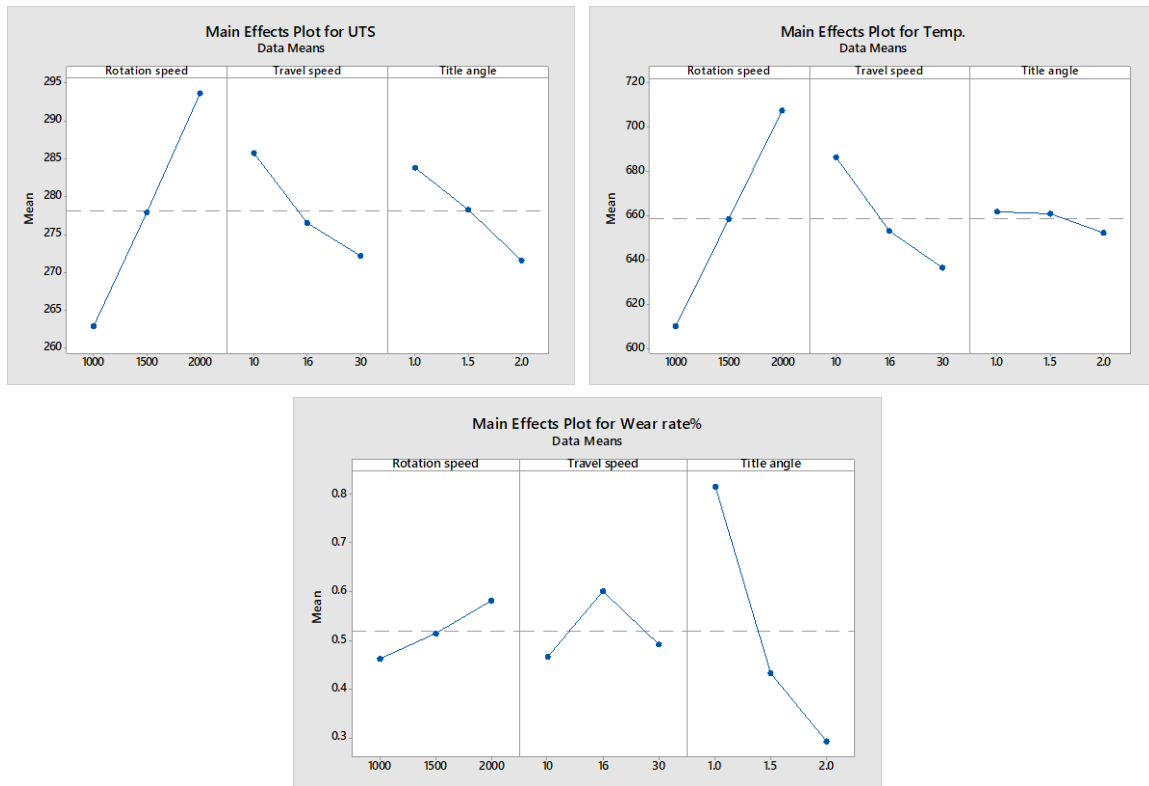


Fig. 8 Plot showing main impacts for rotation speed, travel speed, and tilt angle UTS (b) temperature ($^{\circ}\text{C}$) and (c) tool wear percentage.

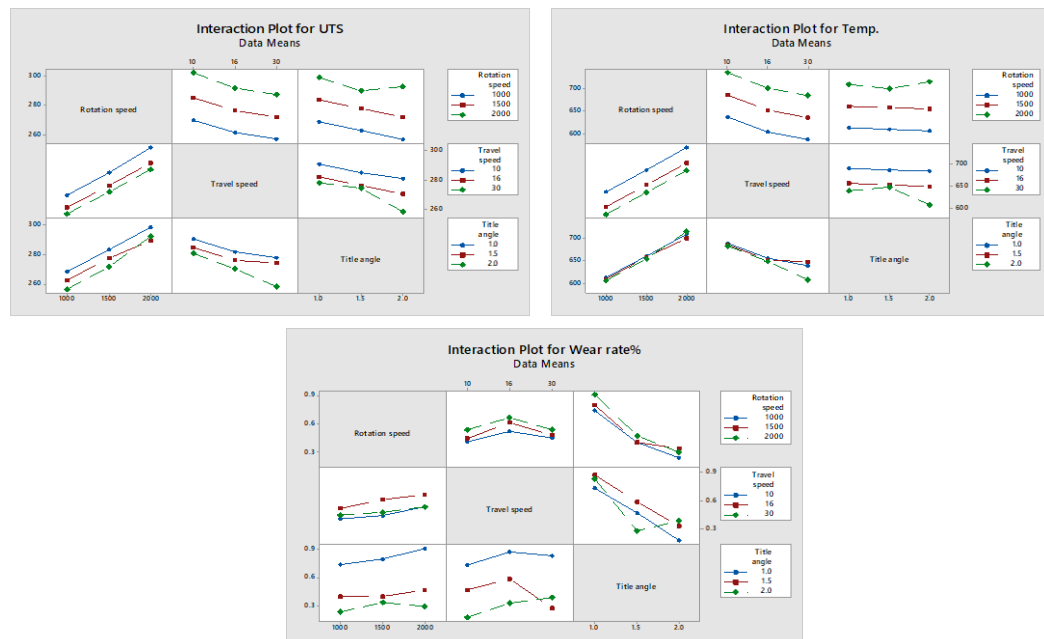


Fig. 9. Interaction of process variables: rotational speed, travel speed, and tilt angle (a) ultimate tensile strength (UTS), (b) temperature ($^{\circ}\text{C}$), and (c) percentage of tool wear.

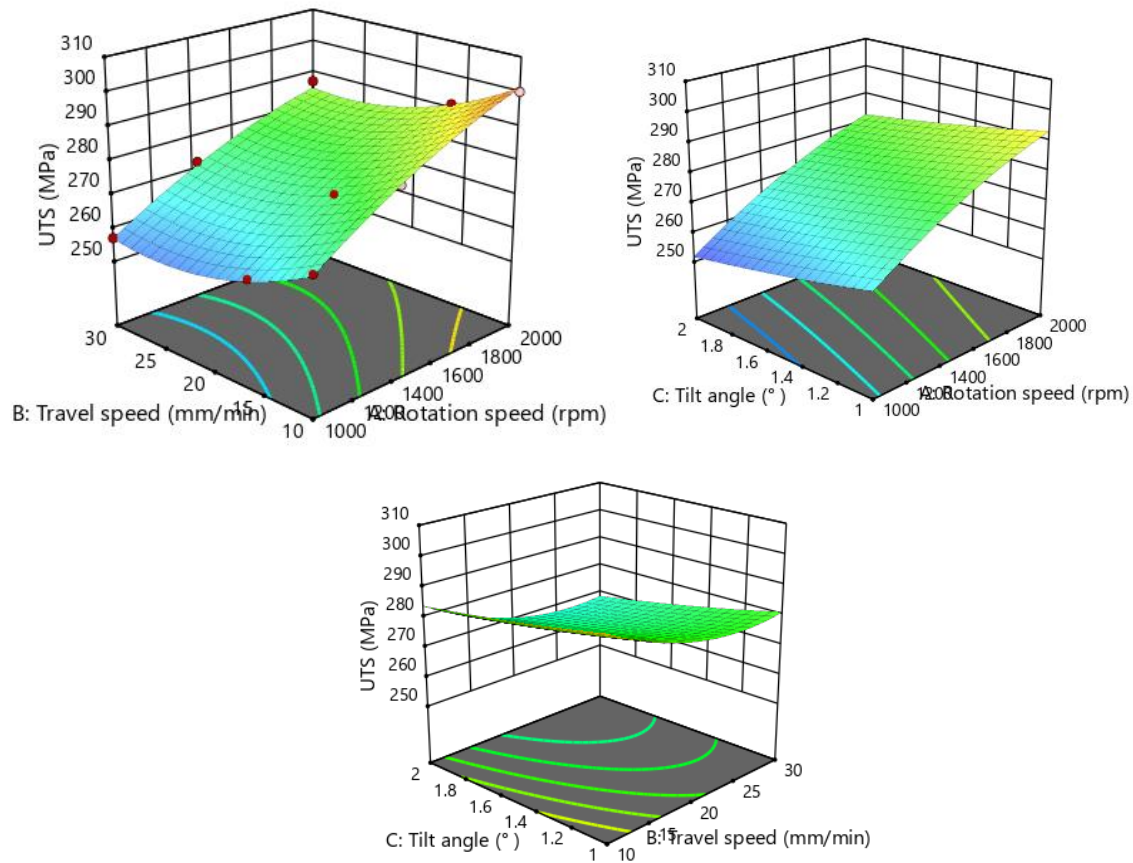


Fig. 10. Contour graphs illustrate the Influence of tilt angle, weld speed, and rotational speed on the ultimate tensile strength of FSW joints.

Researchers have exhaustively examined the impacts of rotation and travel speed, uncovering substantial changes in heat distribution, plastic flow behavior, and joint characteristics. Mourad et al., [31] reported that increased rotation speed and decreased travel speed enhance the mechanical characteristics of the joint. A. Balamurugan et al., [32] have illustrated cases where the contrary holds. The data from Figure 9 indicates that the maximum Temperature increases more substantially at 2000 rpm than at 1000 rpm rotation speed. The plastic flow is obstructed on the advancing side due to an imbalance in FSW. When a more robust alloy is placed on the advancing side, the material will transition to the plastic phase at a reduced temperature. The presence of the harder alloy diminishes plastic flow, leading to a reduction in the maximum Temperature. Figure 11 depicts the interaction among rotation speed, weld travel speed, tilt angle, and Temperature. The Influence of rotation and travel speed on Temperature while sustaining axial force is illustrated in the 3D contour plots (Figure 11a). The impact of rotational speed and axial force on Temperature, with a constant weld transit speed, is illustrated in the 3D contour plots (Figure 11b). The Influence of travel speed and tilt angle on Temperature, with a constant rotational speed, is illustrated in the 3D contour plots (Figure 10 c), aligning with the research conducted, [36 - 42]. The plot analysis indicates that the

peak temperature, attaining an optimal value of 727 degrees Celsius, occurs at a rotation speed of 2000 revolutions per minute and a travel speed of 10 millimeters per minute. The Temperature will either decrease or increase when there is a deviation from the required values of rotational speed and travel speed. Figure 8 depicts the synergistic Effect of tilt angle and rotational speed, with a constant travel speed of 10 mm/min maintained. Examining the 3D plots indicates that the best Temperature is roughly 737 degrees Celsius, with a rotation speed of 2000 revolutions per minute and a tilt angle of 1°.

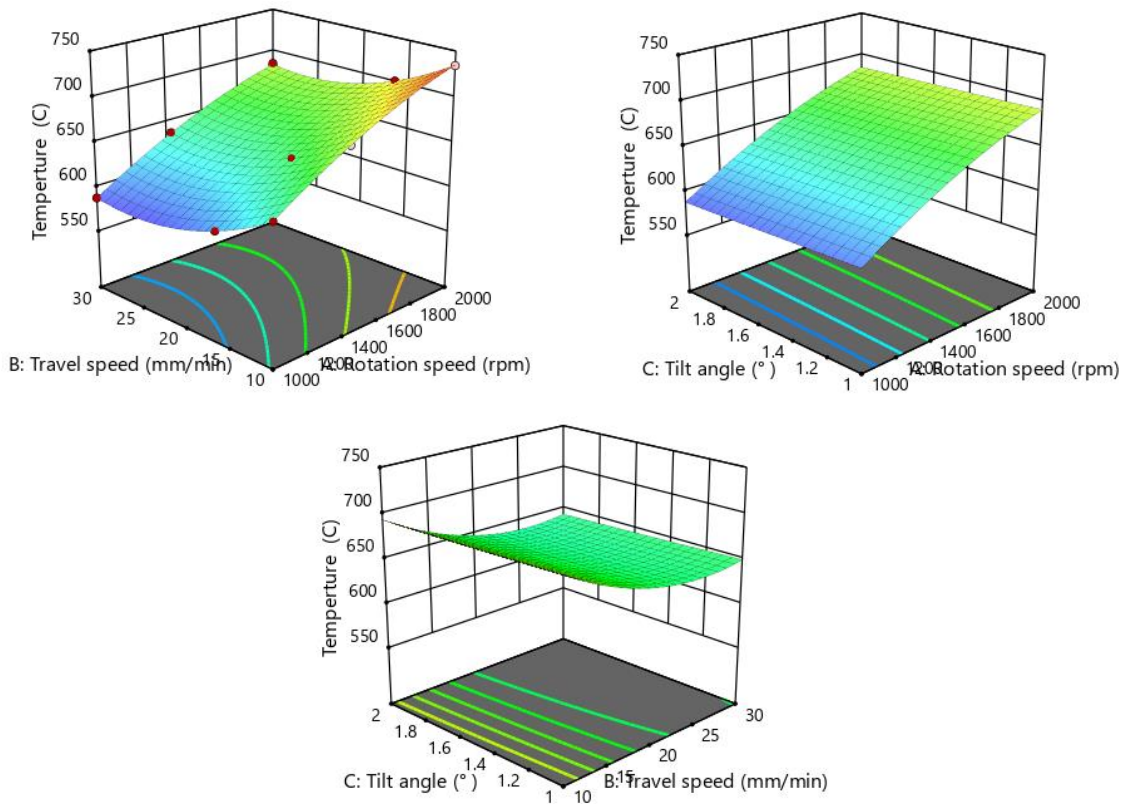


Fig. 11 Contour plots illustrate the Influence of tilt angle, weld speed, and rotating speed on the Temperature of friction stir welds.

Figure 12 depicts the interaction effects of rotation speed, travel speed, and tilt angle on tool wear. The Influence of rotation and travel speed on tool wear while controlling tilt angle is illustrated in the 3D contour plots (Fig. 12 a). The impact of rotation speed and tilt angle on tool wear, with a constant weld transit speed, is illustrated in the 3D contour plots (Fig. 12 b). The Influence of travel speed and tilt angle on tool wear while keeping rotation speed constant is illustrated using 3D contour plots (refer to Fig. 12 c). The analysis indicates that optimal tool wear, at 0.316%, occurs with a rotation speed of 2000 rpm and a travel speed of 10 mm/min. Temperature variations arise in response to deviations from designated rotational and travel speed values. Figure 11 illustrates the effects of tilt angle and rotational speed, with a constant travel speed of 10 mm/min maintained. The analysis of the 3D plots indicates that the

optimal level of tool wear is approximately 0.706 %. The optimal condition is attained with a rotation speed of 2000 rpm and a tilt angle maintained at 1°C.

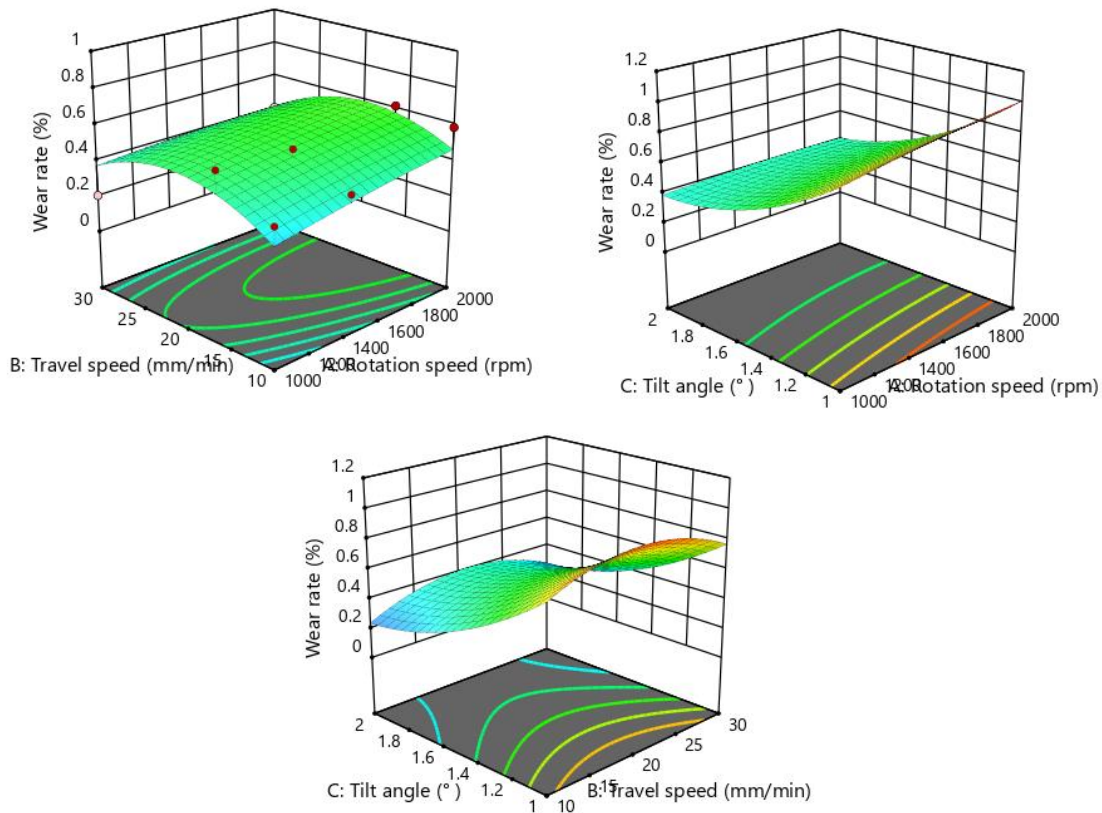


Fig. 12 presents contour plots illustrating the Influence of tilt angle, weld speed, and rotation speed on tool wear in friction stir welding (FSW) joints.

Results of Optimization

Optimization research has identified the optimal welding parameters necessary for achieving the desired mechanical quality of the welded connection, [34]. The selected circumstances were based on particular optimization criteria detailed in Table 5. The experimental findings and Optimization results indicate that optimal ultimate tensile strength (UTS) and Temperature are attained at a rotation speed of approximately 2000 rpm. This suggests that rotation speed predominantly influences the responses relative to other input factors. This aligns with the findings of the study [35]. Figure 13 presents the contour and overlay plots, indicating predictions for the optimal UTS of 306 MPa at a temperature of 737°C. The predictions are derived from optimal welding conditions, which include a rotation speed of 2000 rpm, a travel speed of 10 mm/min, and a tilt angle of 1C. Figure 13 presents the contour and overlay plots, indicating an optimal tool wear prediction of 0.887. The predictions are derived from optimal welding conditions: a rotation speed of 2000 rpm, a travel speed of 10 mm/min, and a tilt angle of 2°.

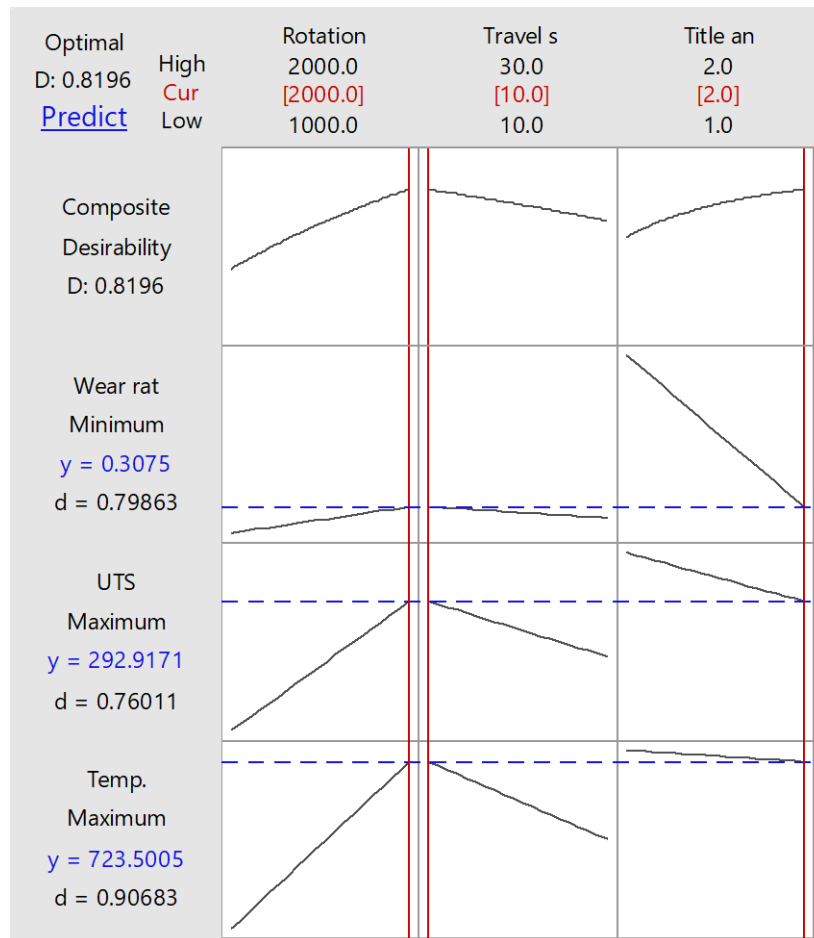


Fig. 13 A map forecasting optimal FSW process parameters.

3.4 Validation of the developed model

The desirability approach model is evaluated for accuracy using experimental data. Table 6 presents the errors for all 27 runs, detailing the actual value, predicted value, and error percentage for the UTS, Temperature, and tool wear. The empirical equations generated by the design expert software are employed to ascertain the expected values, whereas the actual values are derived from experimental procedures. The UTS demonstrates a percentage error range of -0.73% to +1.85%. The error percentages for temperature and tool wear range from -1.312 to +1.21 and -0.204 to +0.186, respectively. The recently developed model has demonstrated high accuracy in predicting UTS, Temperature, and tool wear, aligning closely with experimental data. The model is verified about the anticipated ideal welding conditions. Three confirmation experiments were performed at a rotation speed of 2000 revolutions per minute (rpm), a travel speed of 10 millimeters per minute (mm/min), and a tilt angle of 2 degrees. The anticipated maximum percentage errors for the optimal UTS, Temperature, and tool wear are 1.22%, 1.26%, and 2.779%, respectively.

DISCUSSION

In friction stir welding (FSW), material flow is crucial because it determines the weld quality, defect formation, and thermal distribution in the weld region. Advancing and retreating Sides: The asymmetry in material flow between the advancing side (AS)

and the retreating side (RS) is due to the rotational direction of the tool and its interaction with the base material. This can influence the homogeneity of the weld. **Stirring and plastic deformation:** the rotating tool induces severe plastic deformation in the material, resulting in a "stirring" action. This action causes the plasticized material to flow from the front to the back of the tool, consolidating under the combined effects of pressure and heat. **Tilt angle effect:** The tilt angle creates a downward force that aids material mixing and flow behind the tool, helping eliminate voids and tunnel defects. However, an excessive tilt angle can lead to improper flow and defects like surface grooves or kissing bonds. **Heat generation:** the material flow determines how heat is generated and dissipated in the weld. **Friction between the tool and the workpiece,** combined with plastic deformation of the material, is the primary heat source. **Thermal gradients:** Efficient material flow promotes uniform heat distribution, reducing thermal gradients that can cause internal stresses and defects. **Influence on microstructure:** Temperature affects the material's microstructure by controlling the size and distribution of grains in the weld nugget and adjacent zones. Poor material flow can result in uneven temperature distribution, leading to heterogeneous microstructures.

Tunnel defects, insufficient material flow, or improper consolidation of plasticized material behind the tool can leave voids, often forming tunnel defects. Void formation, Inadequate material stirring, or incorrect tool geometry and process parameters can trap unprocessed material, leading to voids. **Lack of bonding:** Poor material flow can cause improper mixing at the interface, leading to weak bonding.

The parameters you mentioned—10 mm/min travel speed, 2° tilt angle, and 2000 rpm rotational speed—were likely chosen based on their effects on heat generation. **Travel speed (10 mm/min):** A slower travel speed allows more time for the tool to generate heat and adequately plasticize the material. This enhances material flow and reduces the chances of tunnel defects or insufficient bonding. Faster travel speeds may cause insufficient heat generation, leading to poor plasticization and defects like voids or cracks. **Tilt angle (2°):** A slight tilt angle (e.g., 2°) is optimal for directing material flow downward and behind the tool, promoting better consolidation. Larger tilt angles might push the material excessively, causing surface defects or improper material mixing. **Rotational speed (2000 rpm):** High rotational speeds generate significant heat due to increased friction, ensuring effective plasticization of the material. Lower rotational speeds might not generate enough heat, leading to poor material flow and cold welds, while excessively high speeds can cause overheating, grain coarsening, and flash formation.

CONCLUSIONS

This study investigates the experimental and modeling aspects of FSW applied to dissimilar alloys AA6061-T6 and AA6082-T6. It evaluates the effects of rotational speed, travel speed, and tilt angle on critical parameters, including maximum process temperature, UTS, and tool wear. Using Response Surface Methodology (RSM), the research offers the following impactful findings:

1. The three-factorial Box-Behnken design effectively establishes correlations between process parameters (rotational speed, travel speed, and tilt angle) and

responses (UTS, Temperature, and tool wear). This design enabled parameter optimization for UTS, Temperature, and tool wear.

2. Analysis of variance (ANOVA) reveals that rotational speed has the most significant impact on maximum Temperature and UTS, followed by travel speed and tilt angle. A reduction in travel speed leads to lower maximum temperatures.

3. The optimal parameters for achieving 206 MPa UTS, 0.887% tool wear, and 737°C maximum temperature are a rotational speed of 2000 rpm, a travel speed of 10 mm/min, and a tilt angle of 2°. Perturbation and 3D contour plots confirm the dominant Influence of rotational speed.

4. The desirability approach validates the Box-Behnken method, achieving experimental optimal values of 204 MPa UTS, 0.296% tool wear, and 670°C maximum temperature under similar conditions.

These findings provide critical insights into parameter optimization for enhanced weld quality and tool performance in FSW of dissimilar aluminum alloys.

REFERENCES

1. Balamurugan A., Bhuvanewari M., Suresh K. C., Sudha M., "Investigation on the mechanical properties of FSWed AA6063 – T351 aluminum alloy joints", *Materials Today: Proceedings*, (2023), <https://doi.org/10.1016/j.matpr.2023.05.553>.

2. Hewidy A. M., Sabry I., "Underwater friction-stir welding of a stir-cast AA6061-SiC metal matrix composite: Optimization of the process parameters, microstructural characterization, and mechanical properties", *Materials Science Poland*, 40(1)pp. 101-115, (2022), <https://doi.org/10.2478/msp-2022-0013>.

3. Shah L. A., Sonbolestan S., Midawi A. H., Walbridge S. & Gerlich A., "Dissimilar friction stir welding of thick plate AA5052-AA6061 aluminum alloys: effects of material positioning and tool eccentricity", *The International Journal of Advanced Manufacturing Technology*, 105, pp.889–904, (2019), <https://doi.org/10.1007/s00170-019-04287-9>.

4. El-Kassas A. M., Sabry I., Mourad A-H. I., Thekkuden D. T., "Characteristics of Potential Sources - Vertical Force, Torque and Current on Penetration depth for Quality Assessment in Friction Stir Welding of AA 6061 Pipes", *International Review of Aerospace Engineering*, 12(4), pp. 195-207, (2019), DOI: 10.15866/irease.v12i4.16362.

5. Essa A. S., Ahmed M. Z., El-Nikhaily A. E., "An analytical model of heat generation for eccentric cylindrical pin in friction stir welding," *Journal of Materials Research and Technology*, 5(3), pp. 234-240, (2016), <https://doi.org/10.1016/j.jmrt.2015.11.009>.

6. Naghibi H. D., Shakeri M., Hosseinzadeh M., "Neural network and genetic algorithm based modeling and Optimization of tensile properties in FSW of AA 5052 to AISI 304 dissimilar joints", *Transactions of the Indian Institute of Metals*, 69, pp. 891–900, (2016), <https://doi.org/10.1007/s12666-015-0572-2>.

7. Yaduwanshi D., Bag S., "On the effect of tool offset in hybrid-FSW of copper aluminium alloy", *Materials and Manufacturing Processes*, 33(3), pp. 277–287, (2018), DOI: 10.1080/10426914.2017.1279309.

8. Liang Z., Chen K., Wang X., Yao J., Yang Q., Zhang L., Shan A., "Effect of tool offset and tool rotational speed on enhancing mechanical property of Al/Mg dissimilar FSW joints," *Metallurgical and Materials Transactions A*, 44, pp. 3721–3731, (2013), <https://doi.org/10.1007/s11661-013-1700-4>.

9. Ghaffarpour M, Aziz A, Hejazi T. H., "Optimization of friction stir welding parameters using multiple response surface methodology," *Proceedings of the Institution of Mechanical Engineers, Part L: Journal of Materials: Design and Applications*, 231(7), pp. 571-583 (2017), doi:10.1177/1464420715602139.
10. Essa A. S., Ahmed M. Z., Mohamed. Y. A., El-Nikhaily A. E., "An analytical model for the heat generation in friction stir welding," *Modelling and Simulation in Materials Science and Engineering*, 12(1), pp. 234-240, (2003), DOI 10.1088/0965-0393/12/1/013.
11. Su H., Wu C. S., Pittner A., Rethmeier M., "Simultaneous measurement of tool torque, traverse force, and axial force in friction stir welding," *Journal of Manufacturing Processes*, 15(4), pp. 495-500, (2013), <https://doi.org/10.1016/j.jmapro.2013.09.001>.
12. Sabry I., El-Kassas A. M., "An appraisal of characteristic mechanical properties and microstructure of friction," *Journal of Mechanical Engineering and Sciences*, 13(4), pp. 5804-5817, (2019), DOI: <https://doi.org/10.15282/jmes.13.4.2019.07.0463>.
13. Sabry I., El-Kassas A. M., Mourad A-H. I. , Thekkuden D. T. and Qudeiri J. A., "Friction Stir Welding of T-Joints: Experimental and Statistical Analysis. *Journal of Manufacturing and Materials Processing*, 3(38), pp. 1-23, (2019), DOI:10.3390/jmmp3020038.
14. Sabry I., Mourad A-H. I., Thekkuden D. T., "Comparison of Mechanical Characteristics of Conventional and Underwater Friction Stir Welding of AA 6063 Pipe Joints", *International Review of Mechanical Engineering*, 14(1), pp. 64-53, (2020), DOI: 10.15866/ireme.v14i1.17483.
15. Sabry I., Mourad A-H., "Optimization of metal inert gas welded aluminum 6061 pipe parameters using analysis of variance and grey relational analysis", *SN Applied Sciences*, 2(175), (2020), <https://doi.org/10.1007/s42452-020-1943-9>.
16. Yuvaraj K. P., Jose D. M., Sivasankaran R., Kaushik N., Karuppasamy R., Shanthi C., "Mechanical behavior of friction stir welded AA7075-T651 and AA6063-T6 joints - an experimental study", *Materials Today: Proceedings*, 68(6), pp. 2653-2657, (2022), <https://doi.org/10.1016/j.matpr.2022.09.561>.
17. Shah L. H., Guo S., Walbridge S., Gerlich A., "Effect of tool eccentricity on the properties of friction stir welded AA6061 aluminum alloys", *Manufacturing Letters*, 15 (A), pp. 14-17, (2018), <https://doi.org/10.1016/j.mfglet.2017.12.019>.
18. Aliha M. R. M., Shahheidari M., Bisadi M., Akbari M., Hossain S., "Mechanical and metallurgical properties of dissimilar AA6061-T6 and AA7277-T6 joint made by FSW technique", *The International Journal of Advanced Manufacturing Technology* (86), pp. 2551–2565, (2016), DOI: 10.1007/s00170-016-8341-x.
19. Shalin M., Hiten M., "Experimental Analysis on Effect of Tool Transverse Feed, Tool Rotational Speed And Tool Pin Profile Type on Weld Tensile Strength of Friction Stir Welded Joint of AA 6061", *Materials Today: Proceedings*, 5(1), pp. 487-493, (2018), <https://doi.org/10.1016/j.matpr.2017.11.109>.
20. Amatullah M., Jan M., Farooq M., Zargar A. S., Maqbool A., Khan N. Z., "Effect of tool rotational speed on the friction stir welded aluminum alloys: A review, " *Materials Today: Proceedings*, 62 (1), pp. 245-250, (2022), <https://doi.org/10.1016/j.matpr.2022.03.220>.
21. Sabry I., "Exploring the Effect of friction stir welding parameters on the strength of AA2024 and A356-T6 aluminum alloys, *Journal of Alloys and Metallurgical Systems*, 8 (100124) (2024),doi:10.1016/j.jalmes.2024.100124.

22. Sabry I., El-Deeb Mostafa S.S., Hewidy A.M., ElWakilM., "Mechanical and tribological behaviors of friction stir Welding using various strengthening techniques, Journal of Alloys and Metallurgical Systems, 7(100098,2024)(2024),<https://doi.org/10.1016/j.jalmes.2024.100098>.
23. Sabry I., Ahmed Hewidy, Hewidy A.M., "Multi-weld Quality Optimization of Friction Stir Welding for Aluminium Flange Using the Grey-based Taguchi Method, Management and Production Engineering Review, 15(2), pp. 42-56, (2024), DOI: 10.24425/mper.2024.151129
24. Sabry I., Hewidy A.M., AlkhedherM., Mourad A-H., "Analysis of variance and Grey relational analysis application Methods for the Selection and Optimization Problem in 6061-T6 flange Friction Stir Welding Process Parameters, International Journal of Lightweight Materials and Manufacture, 15(2), (2024),<https://doi.org/10.1016/j.ijlmm.2024.06.006>.
26. Sabry I., Hewidy A.M., Naseri M., Mourad A-H., " Optimization of process parameters of metal inert gas welding process on aluminum alloy 6063 pipes using Taguchi-TOPSIS approach, Journal of Alloys and Metallurgical Systems, 7(100085), (2024), <https://doi.org/10.1016/j.jalmes.2024.100085>.
27. Sabry I., Singh V., P., Mourad A-H., Hewidy A.M., " Flange Joining Using Friction Stir Welding and Tungsten Inert Gas Welding of AA6082: A Comparison Based on Joint Performance, International Journal of Lightweight Materials and Manufacture,(2024), <https://doi.org/10.1016/j.ijlmm.2024.05.001>.
28. Khan N. Z., Siddiquee A. N., Khan Z. A, Shihab S. K., "Investigations on tunneling and kissing bond defects in FSW joints for dissimilar aluminum alloys," Journal of Alloys and Compounds, 648, pp. 360-367, (2015), <https://doi.org/10.1016/j.jallcom.2015.06.246>.
29. Sevel P., Jaiganesh V., "Effects of axial force on the mechanical properties of AZ80A Mg alloy during friction stir welding, "Materials Today: Proceedings, 4(2), pp. 1312-1320, (2017), <https://doi.org/10.1016/j.matpr.2017.01.152>.
30. Sahu P. K., Pal S. K., Jain R., "Influence of plate position, tool offset, and tool rotational speed on mechanical properties and microstructures of dissimilar Al/Cu friction stir welding joints," Journal of Materials Processing Technology(235), pp. 55-67, (2016), <https://doi.org/10.1016/j.jmatprotec.2016.04.014>.
31. Srinivasan R., Ramesh A., Athithanambi A., "Effect of Axial Force on Microstructure and Mechanical Properties of Friction Stir Welded Squeeze Cast A413 Aluminium Alloy", Materials Today: Proceedings, 5(5), pp. 13486-13494, (2018). <https://doi.org/10.1016/j.matpr.2018.02.344>.
32. Mishra R. S., Ma Z. Y., "Friction stir welding and processing," Materials Science and Engineering: R: Reports, 50 (1-2), (2005), <https://doi.org/10.1016/j.mser.2005.07.001>.
33. Ramachandran K. K., Murugan N., Shashi K. S., "Friction Stir Welding of Aluminum Alloy AA5052 and HSLA Steel: Mechanical and microstructural characterization of dissimilar friction stir welded butt joints", Welding Journal, 49(4), pp. 291-300, (2015).
34. Sabry I., "Experimental and Statistical Analysis of Possibility Sources - Rotation Speed, Clamping Torque and Clamping Pith for Quality Assessment in Friction Stir Welding, "Management and Production Engineering Review, 12(3), pp. 84–96, (2021), DOI: 10.24425/mper.2021.138533.

35. Verma S., Garg D., Misra J. P., Batra U., "Multi-objective optimum design for FS welded 7039 aluminum alloy considering weld quality issues, "Materials Today Communications,26(102010), (2021), [https://doi.org/ 10.1016/j. mtcomm.2021.102010](https://doi.org/10.1016/j.mtcomm.2021.102010).
36. Lakshminarayanan A. K., Balasubramanian V., "Comparison of RSM with ANFIS in predicting tensile strength of dissimilar friction stir welded AA2024 - AA5083 aluminum alloys", *Procedia Manufacturing*, 37, pp. 555-562, (2019), <https://doi.org/10.1016/j.promfg.2019.12.088>.
37. Mahdavi S., Akhlaghi F., "Effect of SiC content on the processing, compaction behavior, and properties of Al6061/SiC/Gr hybrid composites", *Journal of Materials Science*, 46, pp. 1502 – 1511 (2011), <https://doi.org/10.1007/s10853-010-4954-x>.
38. Miyajima T., Iwai Y., Effects of reinforcements on sliding wear behavior of aluminum matrix composites, *Wear*, 255 (1 - 6), pp. 606 - 616, (2003), [https://doi.org/10.1016/S0043-1648\(03\)00066-8](https://doi.org/10.1016/S0043-1648(03)00066-8).
39. Moustafa S. F., "Wear and wear mechanisms of Al-22%Si/Al₂O₃f composite", *Wear*, 185 (1 - 2), pp. 189 - 195, (1995), [https://doi.org/10.1016/0043-1648\(95\)06607-1](https://doi.org/10.1016/0043-1648(95)06607-1).
40. Wang Q., Kang N., El Mansori M., Yu T., El Hadrouz M., Huang X., Lin X., "Effect of Ti on the microstructure and wear behavior of a selective laser melted AlCu-Mg-Si alloy", *Wear*, 523, pp. 204 - 219, (2023), <https://doi.org/10.1016/j.wear.2023.204790>.
41. Muley A. V., Ruchika D., "Wear and friction (Tribological) characteristic of aluminum-based metal matrix hybrid composite: An overview," *Materials Today: Proceedings*, (2023),<https://doi.org/10.1016/j.matpr.2023.04.143>.
42. Hewidy A. M., Sabry I., "Impact of tool wear on the utmost temperature during the friction stir welding," *Journal of the Egyptian Society of Tribology*, 4, pp. 88 – 105, (2023), DOI: 10.21608/jest.2023.319436